ENCIT 2018

ABCM Associação Brasileira de Engenharia e Ciências Mecânicas

17th Brazilian Congress of Thermal Sciences and Engineering
November 25th-28th, 2018, Águas de Lindóia, SP, Brazil

ENCIT-2018-0825
Numerical study of the influence of spanwise wavelength on the evolution of Görtler vortices for unsteady disturbances

Adriano Sueke Takata
Josuel Kruppa Rogenski
Leandro Franco de Souza
Instituto de Ciências Matemática e Computação, Universidade de São Paulo, Campus São Carlos, Brasil
Av. Trabalhador São Carlense, 400
13566-590, São Carlos - SP
adrianostakata@gmail.com, josuelkr@gmail.com, lefraso@icmc.usp.br

Abstract. *Boundary fluid flow over a concave surface can be unstable to disturbance generating streamwise-oriented counter-rotating vortices. These vortices are known as Gortler vortices. Due to its importance in the engineering industry, there are several studies carried out on this subject. Some recent studies are focus on the development of unsteady disturbances. In the present work, the evolution of unsteady disturbances is studied through the Direct Numerical Simulation (DNS). The unsteady disturbances are inserted through suction and blowing technique. The results indicate that the spanwise wavelength has a great influence on the evolution of Görtler vortices and also that the growth rate is reduced with the increase of disturbance frequency.*

Keywords: *Unsteady Disturbance, Görtler Vortices, Direct Numerical Simulation, Non-linear Analysis, Spanwise Wavelength*

1. INTRODUCTION

The instability in boundary layers on the concave surface may lead to the formation of streamwise-oriented counter-rotating vortices (Saric, 1994), as shows the in Fig. 1. The generation of these vortices occurs because of the imbalance of centrifugal and inertial forces. This type of vortex was studied initially by Görtler (1941) which bears his name. The Görtler vortices appear in several aerodynamic flows as turbine blades or airfoils, so it is of great importance for the aeronautical industry.

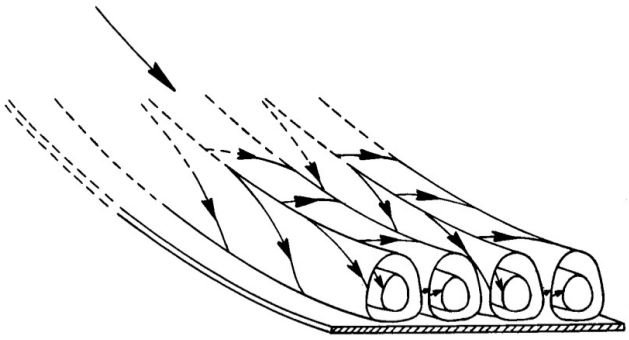

Figure 1. Görtler vortices. Source Görtler (1941)

The vortices can be generated both experimentally and numerically by introducing infinitesimal disturbances in the flow. These disturbances can be inserted by the external factors such as surface roughness, acoustic vibrations among other (Denier *et al.*, 1991) or by an internal factor as wall-transpiration (suction and blowing strip) (Souza *et al.*, 2004). Moreover, the disturbances are also classified herein as steady and unsteady. The researchers considered only the steady case until 2010. Boiko *et al.* (2010) published the first experimental and theoretical article for the unsteady disturbances. They made theoretical investigation through the linear-stability theory (LST). Marensi and Ricco (2017) and Xu *et al.* (2017) used a direct numerical simulation (DNS) and a similar mathematical formulation to study boundary layers on a concave surface inserting unsteady perturbation through the free-stream vortical disturbance (FSVD). The difference between them is that Marensi and Ricco (2017) focus on wall-based control results and Xu *et al.* (2017) focus on the secondary instability of the vortices.

The goal of the present work is to investigate the influence of the spanwise wavelength in the unsteady Görtler flows

through direct numerical simulations when the unsteady disturbances are inserted through a suction and blowing strip.

2. MATHEMATICS FORMULATION

The governing equations are the incompressible and unsteady Navier-Stokes equations and heat transfer transport equation in the curvilinear system being x streamwise, y wall-normal and z spanmwise coordinates with Lamé coefficients $h_1 = 1 - yk_c$ and $h_2 = h_3 = 1$ (Floryan and Saric, 1982), where $k_c = L/R$ is the wall curvature being L the reference length and R the radius of curvature. Furthermore, it is used Floryan's order of magnitude analysis to eliminate curvature terms of high order. The methodologies utilized to simplify the solution of governing equations are: (a) the vorticity-velocity formulation to eliminate the pressure terms; and (b) the vorticity, velocity and temperature components are decomposed in baseflow and perturbation parts. The baseflow is assumed to be two-dimensional and the system of perturbation equations is given by:

$$\frac{\partial \omega_x}{\partial t} + \frac{\partial a}{\partial y} - \frac{\partial b}{\partial z} + \frac{Go^2}{\sqrt{Re}}\frac{\partial d}{\partial z} = \frac{1}{Re}\nabla^2\omega_x \tag{1}$$

$$\frac{\partial \omega_y}{\partial t} + \frac{\partial c}{\partial z} - \frac{\partial a}{\partial x} = \frac{1}{Re}\nabla^2\omega_y \tag{2}$$

$$\frac{\partial \omega_z}{\partial t} + \frac{\partial b}{\partial x} - \frac{\partial c}{\partial y} - \frac{Go^2}{\sqrt{Re}}\frac{\partial d}{\partial x} = \frac{1}{Re}\nabla^2\omega_z \tag{3}$$

$$\frac{\partial u}{\partial x} + \frac{\partial v}{\partial y} + \frac{\partial w}{\partial z} = 0 \tag{4}$$

$$\frac{\partial^2 u}{\partial x^2} + \frac{\partial^2 u}{\partial z^2} = -\frac{\partial \omega_y}{\partial z} - \frac{\partial^2 v}{\partial x \partial y} \tag{5}$$

$$\frac{\partial^2 v}{\partial x^2} + \frac{\partial^2 v}{\partial y^2} + \frac{\partial^2 v}{\partial z^2} = -\frac{\partial \omega_z}{\partial x} + \frac{\partial \omega_x}{\partial z} \tag{6}$$

$$\frac{\partial^2 w}{\partial x^2} + \frac{\partial^2 w}{\partial z^2} = +\frac{\partial \omega_y}{\partial x} - \frac{\partial^2 v}{\partial y \partial z} \tag{7}$$

$$\frac{\partial \theta}{\partial t} + \frac{\partial e}{\partial x} + \frac{\partial f}{\partial y} + \frac{\partial g}{\partial z} = \frac{1}{Re\,Pr}\nabla^2\theta, \tag{8}$$

where the variables ($u,\ v,\ w,\ \omega_x,\ \omega_y,\ \omega_z,\ \theta$) are the disturbance velocity, vorticity and temperature component. The Reynolds, Görtler and Prandtl numbers are defined as $Re = U_\infty L/\nu$, $Go = (k_c\sqrt{Re})^{1/2}$ and $Pr = \nu/\alpha$ respectively, where U_∞ is freestrem velocity, ν is kinematic viscosity and α is the thermal diffusivity of the fluid. In addition, the other variables are defined as (when a bar on top of the variables implies baseflow quantities):

$$a = \omega_x(\bar{v} + v) - \omega_y(\bar{u} + u),$$

$$b = \omega_z u + \omega_z \bar{u} + \bar{\omega}_z u - \omega_x w,$$

$$c = \omega_y w - \bar{\omega_z} v - \omega_z \bar{v} - \omega_z v,$$

$$d = 2\bar{u}u + u^2.$$

$$e = \bar{u}\theta + u\bar{\theta} + u\theta$$

$$f = \bar{v}\theta + v\bar{\theta} + v\theta$$

$$g = w(\bar{\theta} + \theta)$$

In order to solve the Eq. (1)-(8) it is necessary to specify the boundary conditions. However, they will not be addressed here with exception of the disturbance insertion region where it will be described in the next section. The boundary conditions used in this work can be found in (Malatesta *et al.*, 2017).

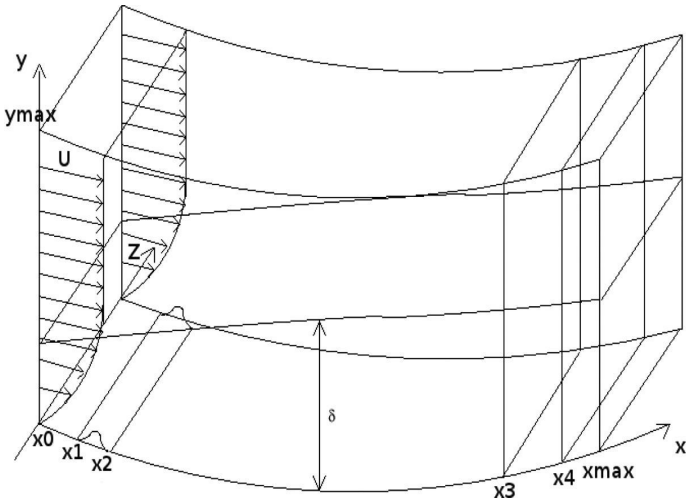

Figure 2. Computational domain, where the inflow is at $x = x_0$, the disturbance is introduced at $x_1 \leq x \leq x_2$, the region of interest is localized at $x_2 \leq x \leq x_3$, the damping region is at $x_3 \leq x \leq x_4$ and the outflow is the $x = x_{\max}$. Source (Malatesta *et al.*, 2017).

3. NUMERICAL FORMULATION

The Eqs.(1)-(8) are solved numerically in the domain illustrated in Fig. 2, where the inflow is at $x = x_0$, the disturbance is introduced at $x_1 \leq x \leq x_2$, the region of interest is localized at $x_2 \leq x \leq x_3$, the damping region is at $x_3 \leq x \leq x_4$ and the outflow is at $x = x_{\max}$.

The flow can be taken periodic in the spanwise direction, so the Eqs. (1)-(8) are approximated by the linear combination of $K + 1$ Fourier modes, for example:

$$u(x, y, z, t) = \sum_{k=0}^{K} U_k(x, y, t) e^{-i\beta_k z}, \tag{9}$$

where $\beta_k = 2\pi k/\lambda_z$ is the spanwise wavenumber and λ_z is the spanwise wavelength. Therefore, it obtains the following system of equations:

$$\frac{\partial \Omega_{xk}}{\partial t} + \frac{\partial A_k}{\partial y} + i\beta_k B_k - i\beta_k \frac{Go^2}{\sqrt{Re}} D_k = \frac{1}{Re} \nabla_k^2 \Omega_{xk}, \tag{10}$$

$$\frac{\partial \Omega_{yk}}{\partial t} - i\beta_k C_k - \frac{\partial A_k}{\partial x} = \frac{1}{Re} \nabla_k^2 \Omega_{yk}, \tag{11}$$

$$\frac{\partial \Omega_{zk}}{\Omega t} + \frac{\partial B_k}{\partial x} - \frac{\partial C_k}{\partial y} - \frac{Go^2}{\sqrt{Re}} \frac{\partial D_k}{\partial x} = \frac{1}{Re} \nabla_k^2 \Omega_{zk}, \tag{12}$$

$$\frac{\partial U_k}{\partial x} + \frac{\partial V_k}{\partial y} - i\beta_z W_k = 0 \tag{13}$$

$$\frac{\partial^2 U_k}{\partial x^2} - \beta_k^2 U_k = i\beta_k \Omega_{yk} - \frac{\partial^2 V_k}{\partial x \partial y}, \tag{14}$$

$$\frac{\partial^2 V_k}{\partial x^2} + \frac{\partial^2 V_k}{\partial y^2} - \beta_k^2 V_k = -\frac{\partial \Omega_{yk}}{\partial x} - i\beta_k \Omega_{xk}, \tag{15}$$

$$\frac{\partial^2 W_k}{\partial x^2} - \beta_k^2 W_k = \frac{\partial \Omega_{yk}}{\partial x} + i\beta_k \frac{\partial V_k}{\partial y}, \tag{16}$$

$$\frac{\partial \Theta_k}{\partial t} + \frac{\partial E_k}{\partial x} + \frac{\partial F_k}{\partial y} - i\beta_k G_k = \frac{1}{Re\ Pr} \nabla^2 \Theta_k \tag{17}$$

where

$$\nabla_k^2 = \left(\frac{\partial^2}{\partial x^2} + \frac{\partial^2}{\partial y^2} - \beta_k^2 \right).$$

In the disturbance insertion region ($x_1 \leq x \leq x_2$), the boundary conditions will be modified introducing unsteady disturbance instead of steady disturbance. The perturbation are inserted through suction and blowing of mass at V_k velocity along the streamwise direction with $k = 1$. Thus, this boundary condition is given by following the function:

$$V_1(x, 0, t) = \begin{cases} A \sin^3(\epsilon) \cos(\omega t) & \text{for} \quad x \in [x_1, x_2] \\ 0 & \text{for} \quad x \in [x_0, x_1) \cup (x_2, x_{max}] \end{cases}, \tag{18}$$

where A is the amplitude, $\epsilon = \pi(x - x_1)/(x_2 - x_1)$, $\omega = 2\pi f L/U_\infty$ and f is the frequency.

The code used for the simulation is the High Order Parallel Code (HOPe) being "High Order" due to high order that the temporal and spatial derivatives are approximated by the high order compact finite difference-schemes (Lele, 1992) and classical 4th order Runge-Kutta integration schemes (Ferziger and Peric, 2012), receptively and the "Parallel" because the code is parallelized using the domain decomposition technique in the streamwise direction and the communication is made by MPI library. In addition, the wall-normal direction is used the stretching of mesh. For more details about HOPe see (Souza, 2017).

4. RESULTS

The verification is done considering the steady disturbance case, that is when $f = 0$ Hz and the results are compared with of Souza (2017), where the radius of curvature is $R = 3.2$ m, and the freestream velocity is $U_\infty = 5.0$ m/s. The kinematic viscosity considered is $\nu = 1.509 \times 10^{-5}$ m^2/s and reference length used is $L = 0.1$ m. Thus, the following values for the Reynolds and Görtler number are $Re = 33124.0$ and $Go = 2.385$ respectively.

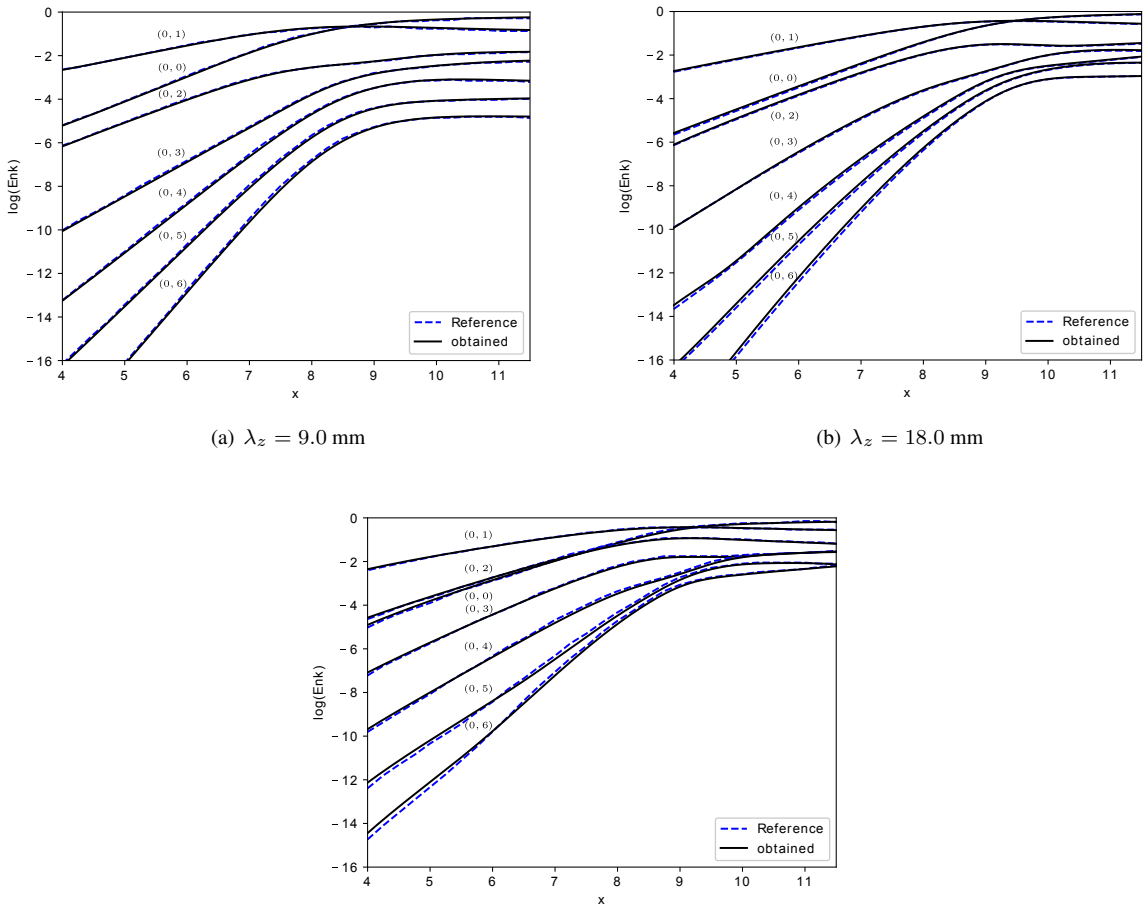

(a) $\lambda_z = 9.0$ mm

(b) $\lambda_z = 18.0$ mm

(c) $\lambda_z = 36.0$ mm

Figure 3. The disturbance energy (19) for the following spanwise wavelength:(a) $\lambda_z = 9.0$ mm, (b) $\lambda_z = 18.0$ mm and (c) $\lambda_z = 36.0$ mm.

The distance between two consecutive points at streamwise direction is $dx = 1.0 \times 10^{-2}$ and the initial spacing at wall-normal direction is $dy = 8.0 \times 10^{-4}$ with stretching of 1%. The temporal step is $dt = 2.0 \times 10^{-3}$. The number of points used in the streamwise and wall-normal direction is Nx $= 1345$ and Ny $= 201$ respectively. In the spanwise

direction is adopted 11 Fourier modes and it is considered 32 points in the physical space. The disturbances are introduced between at $x_1 = 1.2$ and $x_2 = 1.52$ and the damping region is bewteen at $x_3 = 13.9$ and $x_4 = 14.4$.

The metric used for steady case is the disturbance energy proposed by Li and Malik (1995) and it is defined:

$$En_k = \begin{cases} \frac{1}{2}\int_0^\infty (|U_k|^2 + |W_k|^2)dy & \text{for} \quad k = 0. \\ \int_0^\infty (|U_k|^2 + |V_k|^2 + |W_k|^2)dy & \text{if} \quad k > 0 \end{cases} \tag{19}$$

The spanwise wavelengths considered are $\lambda_z = 9.0,\ 18.0$ and 36.0 mm with their respective values for the wavelength of the fundamental Fourier mode $\Lambda = (U_\infty \lambda_z/\nu)(\lambda_z/R)^{1/2} = 158.099,\ 447.173$ and 1264.799. In addition, the following amplitudes $A = 3.9 \times 10^{-3}, 1.35 \times 10^{-3}$ and 4.1×10^{-5} are considered respectively.

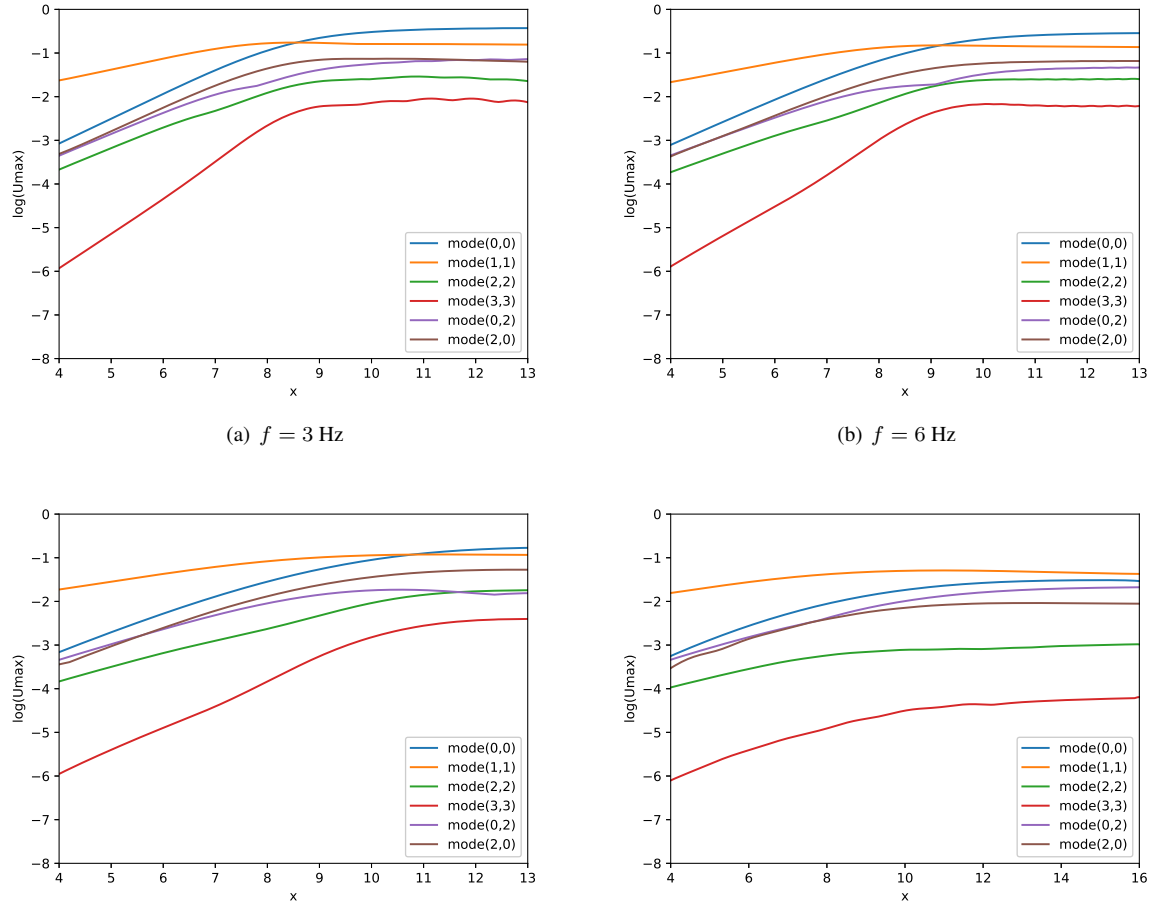

(a) $f = 3$ Hz (b) $f = 6$ Hz

(c) $f = 9$ Hz (d) $f = 12$ Hz

Figure 4. The maximum streamwise velocity amplitude in the yz-plane with the $\lambda_z = 9.0$ mm for the following frequencies:(a) $f = 3$ Hz, (b) $f = 6$ Hz, (c) $f = 9$ Hz and $f = 12$ Hz.

The results are shown in Fig. 3, where the dash line is reference solution (Souza, 2017) and the solid line is the solution obtained by simulation. It can be observed a good agreement between the results for the three spanwise wavelengths. The saturation point is the intersection between mode (0,0) and the mode where is introduced the disturbance. The disturbance energy for $\lambda_z = 9.0$ mm is presented in Fig 3(a), where the saturation point is in $x \approx 8.75$. In Fig. 3(b), for $\lambda_z = 18.0$ mm, the saturation point is in $x \approx 9.25$. Finally, in Fig. 3(c), the saturation point for $\lambda_z = 36.0$ mm is at the same point that for $\lambda_z = 18.0$ mm. It can be observed that the energy of all modes increases in the saturation region as the spanwise wavelength increases.

In unsteady disturbance simulations, the number of points in the streamwise direction is the only parameter changed. Moreover, four different frequencies are considered $f = 3,\ 6,\ 9$ and 12 Hz with the following values for $\omega = 0.3769,\ 0.7539,\ 1.1309$ and 1.5079. The evolution of the unsteady disturbances in the flow is analyzed through a Fourier analysis in time. Thus for a Fourier mode, the vorticity, velocity and temperature components depend only on the variables x and y and they have the following notation: $\Phi_{m,k}(x, y)$, where Φ is the flow properties and the indices m and k are the temporal

and spacial Fourier modes respectively. The metric used to analyze the results is given by:

$$Umax_{m,k} = \max_{y} U_{m,k}(x, y) \tag{20}$$

In the $\lambda_z = 9.0$ mm, it is used Nx=1385 for $f = 3,\ 6$ and 9 Hz and Nx $= 1615$ for $f = 12$ Hz. In the Fig. 4, it is presented the results with the Eq. (20) for the four different frequencies. Through the three first graphs of the Fig. 4, it can be observed that the saturation point is further away from the origin as the frequency increases. However, the saturation point does not appear for $f = 12$ Hz, even with a larger domain. Moreover, when $f = 3,\ 6$ and 9 Hz the mode $(2, 0)$ is more relevant than $(0, 2)$, but for $f = 12$ Hz has the opposite occurs.

For the $\lambda_z = 18.0$ mm case, it is used Nx $= 1385$ for $f = 3$ and 6 Hz, Nx $= 1625$ for $f = 9$ Hz and Nx $= 1865$ for $f = 12$ Hz. In Fig. 5, it is shown the results obtained by simulation which observes the same behavior of the saturation point to the $\lambda_z = 9.0$ mm case for $f = 3,\ 6$ and 9 Hz. When $f = 12$ Hz the intersection between the modes $(0, 0)$ and $(1, 1)$ can be observed, but this intersection happens before the $f = 9$ Hz. It may note that the region where mode $(0, 2)$ is dominant over $(0, 0)$ grows as the frequency increases for $f = 3,\ 6$ and 9 Hz. However, this fact is not true for $f = 12$ Hz.

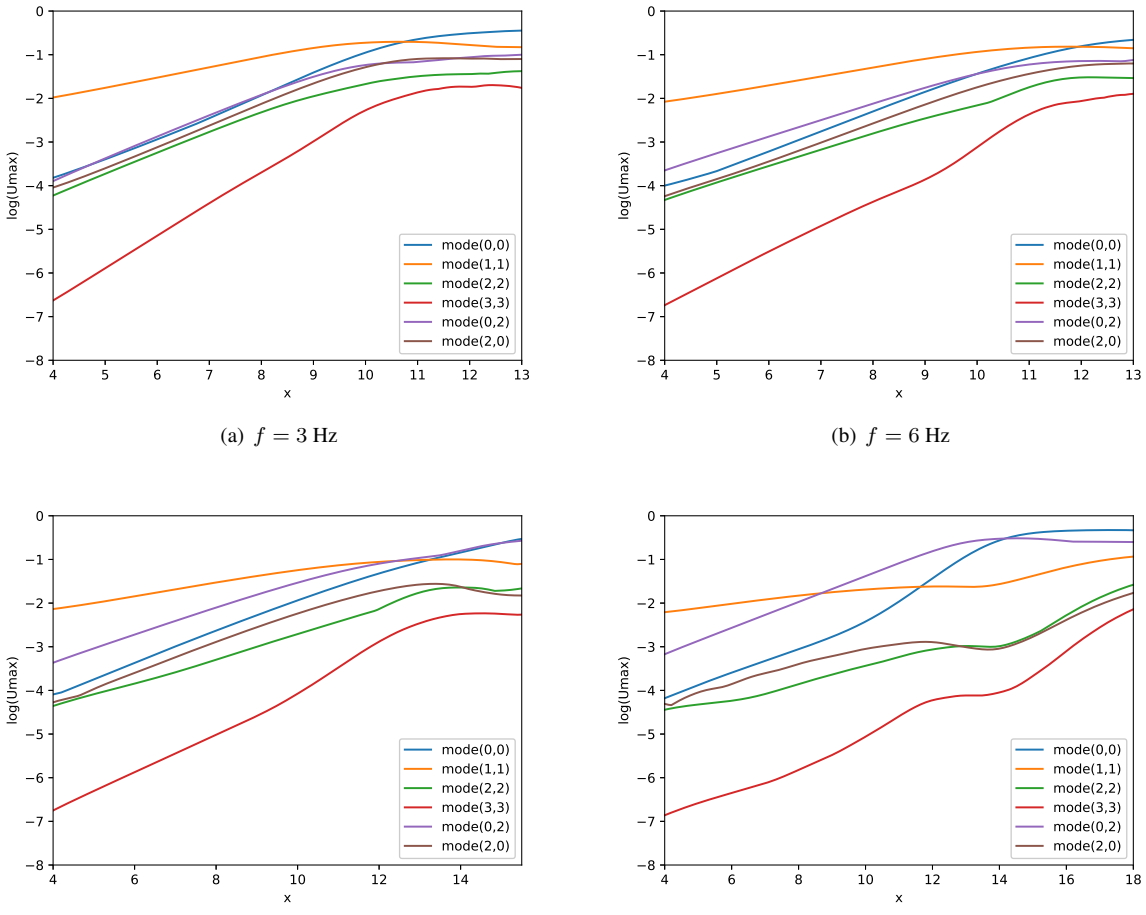

(a) $f = 3$ Hz (b) $f = 6$ Hz

(c) $f = 9$ Hz (d) $f = 12$ Hz

Figure 5. The maximum streamwise velocity amplitude in the yz-plane with spanwise wavelength $\lambda_z = 18.0$ mm for the following frequencies:(a) $f = 3$ Hz, (b) $f = 6$ Hz, (c) $f = 9$ Hz and $f = 12$ Hz.

Finally, in case of $\lambda_z = 36.0$ mm, it is adopted Nx $= 1865$ for $f = 3$ Hz, Nx $= 2105$ for $f = 6$ and 9 Hz and Nx $= 2425$ for $f = 12$ Hz. In Fig. 6, it is presented the results obtained by simulation. In Fig. 6, it is presented the results obtained by simulation. Note that there is no relation between the increase of the frequency and the distance of the saturation point with the origin. Note also that with the exception $f = 3$ Hz case, the modes continue to grow throughout the domain without presenting a neutral region, in other words, a region where there is no growth and decrease of the maximum streamwise velocity. Similarly to the case of $\lambda_z = 18.0$ mm, the mode $(0, 2)$ is dominant over the mode $(0, 0)$ in all cases. Moreover, the mode $(1, 1)$ decreases for $f = 12$ Hz.

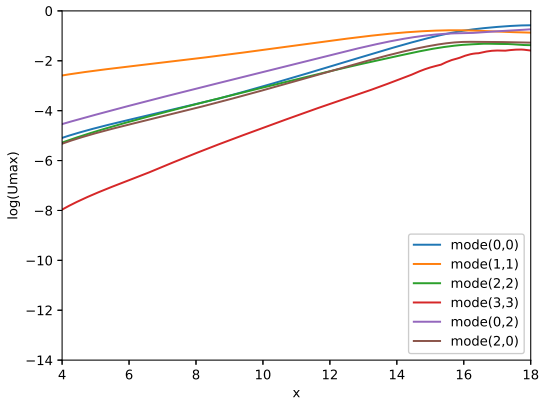

(a) $f = 3$ Hz

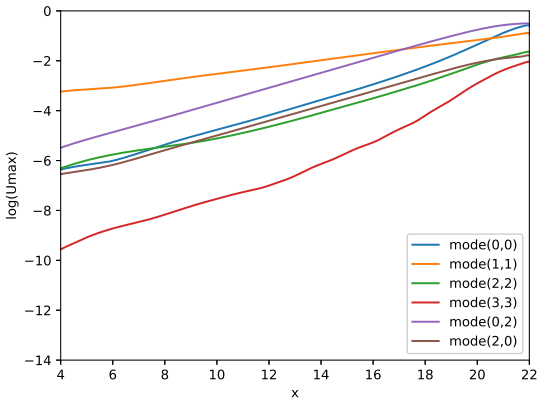

(b) $f = 6$ Hz

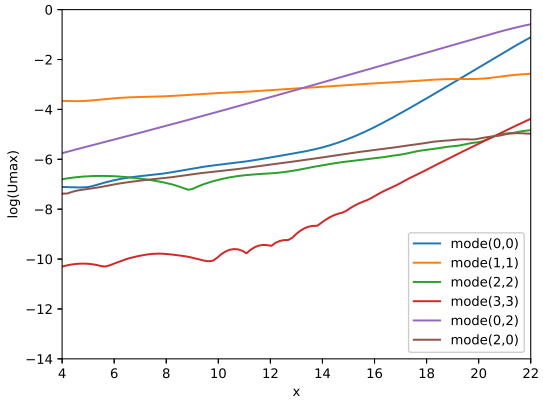

(c) $f = 9$ Hz

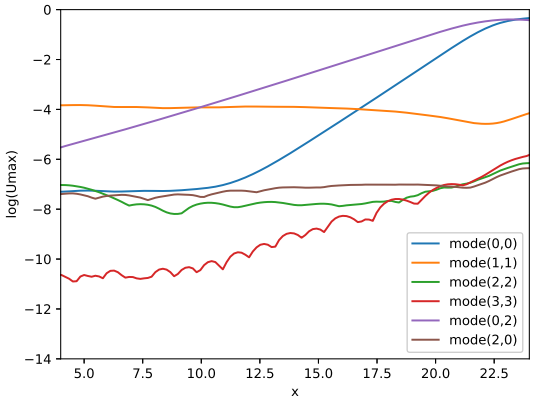

(d) $f = 12$ Hz

Figure 6. The maximum streamwise velocity amplitude in the yz-plane with spanwise wavelength $\lambda_z = 36.0$ mm for the following frequencies:(a) $f = 3$ Hz, (b) $f = 6$ Hz, (c) $f = 9$ Hz and $f = 12$ Hz.

5. CONCLUSION

In the present work, the behavior of unsteady Görtler vortices was analyzed by means of numerical simulation. The adopted code was verified by comparison with other numerical simulation. For the unsteady simulation, Görtler vortices were analyzed using three spanwise wavelength and four disturbances frequencies. The results show that the mode (0,2) becomes more dominant as the frequency increases. The mode (1,1) showed to be more dominant for lower frequency. The results showed also that the saturation point moves in the streamwise direction as the frequency or the spanwise wavelength increase.

6. ACKNOWLEDGEMENTS

We thank CAPES for financial support and ICMC-USP for technical support and infrastructure. Research carried out using the computational resource of the Center for Mathematical Applied to Industry (CeMEAI) funded by FAPESP (Process Number 2013/07375-0).

7. REFERENCES

Boiko, A., Ivanov, A., Kachanov, Y.S. and Mischenko, D., 2010. "Steady and unsteady görtler boundary-layer instability on concave wall". *European Journal of Mechanics-B/Fluids*, Vol. 29, No. 2, pp. 61–83.

Denier, J.P., Hall, P. and Seddougui, S.O., 1991. "On the receptivity problem for görtler vortices: vortex motions induced by wall roughness". *Phil. Trans. R. Soc. Lond. A*, Vol. 335, No. 1636, pp. 51–85.

Ferziger, J.H. and Peric, M., 2012. *Computational methods for fluid dynamics*. Springer Science & Business Media.

Floryan, J.M. and Saric, W.S., 1982. "Stability of gortler vortices in boundary layers". *AIAA journal*, Vol. 20, No. 3, pp. 316–324.

Görtler, H., 1941. "Instabilität laminarer grenzschichten an konkaven wänden gegenüber gewissen dreidimensionalen störungen". *ZAMM - Journal of Applied Mathematics and Mechanics / Zeitschrift für Angewandte Mathematik und Mechanik*, Vol. 21, No. 4, pp. 250–252.

Lele, S.K., 1992. "Compact finite difference schemes with spectral-like resolution". *Journal of computational physics*, Vol. 103, No. 1, pp. 16–42.

Li, F. and Malik, M.R., 1995. "Fundamental and subharmonic secondary instabilities of görtler vortices". *Journal of Fluid Mechanics*, Vol. 297, pp. 77–100.

Malatesta, V., Rogenski, J.K. and Souza, L.F., 2017. "Heat transfer enhancement via görtler flow with spatial numerical simulation". *International Journal of Numerical Methods for Heat & Fluid Flow*, Vol. 27, No. 1, pp. 189–209.

Marensi, E. and Ricco, P., 2017. "Growth and wall-transpiration control of nonlinear unsteady görtler vortices forced by free-stream vortical disturbances". *Physics of Fluids*, Vol. 29, No. 11, p. 114106.

Saric, W.S., 1994. "Görtler vortices". *Annual Review of Fluid Mechanics*, Vol. 26, No. 1, pp. 379–409.

Souza, L.F., 2017. "On the odd and even secondary instabilities of görtler vortices". *Theoretical and Computational Fluid Dynamics*, Vol. 31, No. 4, pp. 405–425.

Souza, L.F., Mendonça, M.T., Medeiros, M.A.F. and Kloker, M., 2004. "Seeding of görtler vortices through a suction and blowing strip". *Journal of the Brazilian Society of Mechanical Sciences and Engineering*, Vol. 26, No. 3, pp. 269–279.

Xu, D., Zhang, Y. and Wu, X., 2017. "Nonlinear evolution and secondary instability of steady and unsteady görtler vortices induced by free-stream vortical disturbances". *Journal of Fluid Mechanics*, Vol. 829, pp. 681–730.

8. RESPONSIBILITY NOTICE

The authors are the only responsible for the printed material included in this paper.